CDDpress

www.nature.com/cdd

ARTICLE

Check for updates

dsDNA-induced AIM2 pyroptosis halts aberrant inflammation during rhabdomyolysis-induced acute kidney injury

Chintogtokh Baatarjav[1,2], Takanori Komada[1,2]✉, Tadayoshi Karasawa[1], Naoya Yamada[1], Ariunaa Sampilvanjil[1], Takayoshi Matsumura[1] and Masafumi Takahashi[1]✉

Rhabdomyolysis is a severe condition that commonly leads to acute kidney injury (AKI). While double-stranded DNA (dsDNA) released from injured muscle can be involved in its pathogenesis, the exact mechanism of how dsDNA contributes to rhabdomyolysis-induced AKI (RIAKI) remains obscure. A dsDNA sensor, absent in melanoma 2 (AIM2), forms an inflammasome and induces gasdermin D (GSDMD) cleavage resulting in inflammatory cell death known as pyroptosis. In this study using a mouse model of RIAKI, we found that *Aim2*-deficiency led to massive macrophage accumulation resulting in delayed functional recovery and perpetuating fibrosis in the kidney. While *Aim2*-deficiency compromised RIAKI-induced kidney macrophage pyroptosis, it unexpectedly accelerated aberrant inflammation as demonstrated by $CXCR3^{+}CD206^{+}$ macrophage accumulation and activation of TBK1-IRF3/NF-κB. Kidney macrophages with intact AIM2 underwent swift pyroptosis without IL-1β release in response to dsDNA. On the other hand, dsDNA-induced *Aim2*-deficient macrophages escaped from swift pyroptotic elimination and instead engaged STING-TBK1-IRF3/NF-κB signalling, leading to aggravated inflammatory phenotypes. Collectively, these findings shed light on a hitherto unknown immunoregulatory function of macrophage pyroptosis. dsDNA-induced rapid macrophage cell death potentially serves as an anti-inflammatory program and determines the healing process of RIAKI.

Cell Death & Differentiation (2022) 29:2487–2502; https://doi.org/10.1038/s41418-022-01033-9

INTRODUCTION

Rhabdomyolysis is a pathological condition characterized by skeletal muscle breakdown, which elicits the release of intracellular contents into blood circulation. Kidneys are commonly affected, and this manifests as rhabdomyolysis-induced acute kidney injury (AKI) (RIAKI). Patients with this life-threatening complication commonly require kidney replacement therapy, and 10–14% of patients die during hospitalization [1–3]. Moreover, recent evidence reveals that there is a significant risk that AKI will transition to chronic kidney disease (CKD) after a single episode of RIAKI [3]. Intramuscular contents including danger-associated molecular patterns (DAMPs), such as myoglobin and heme, are considered to be nephrotoxic and contribute to the onset of RIAKI. Recently, endogenously released double-stranded DNA (dsDNA) has also been suggested to play a role in its pathogenesis [4]. However, the precise mechanism by which dsDNA contributes to kidney inflammation in this syndrome remains largely unknown.

The presence of dsDNA in the cytosol is recognized by a plethora of pattern recognition receptors (PRRs), leading to an innate immune response and/or cell death. Absent in melanoma 2 (AIM2) is an inflammasome-forming DNA-sensing PRR [5, 6]. Inflammasomes are innate immune pathways that regulate inflammation and necrotic cell death called pyroptosis. AIM2 is comprised of one N-terminal PYD domain and one C-terminal HIN domain, which preferentially binds to dsDNA in a non-sequence-specific manner. Upon activation, AIM2 assembles apoptosis-associated speck-like protein containing a CARD (ASC) molecules via homotypic PYD-PYD interactions and then recruits pro-inflammatory caspase-1. Proximity-induced caspase-1 activation triggers the maturation of interleukin (IL)-1β/IL-18 and the cleavage of gasdermin D (GSDMD), providing inflammation and pyroptosis. In CKD, the release of dsDNA from necrotic cells has been implicated in activation of the AIM2 inflammasome [7]. Moreover, we previously reported that another inflammasome-forming PRR, NLRP3, is involved in the pathogenesis of RIAKI [8]. These observations led us to hypothesize that the AIM2 inflammasome would recognize extracellular dsDNA during RIAKI and contribute to its consequences. On the other hand, numerous non-AIM2 DNA-sensing PRRs have been identified to date. Most of them, such as cyclic GMP-AMP synthase (cGAS), induce the transcription of type I interferons (IFNs) and inflammation by activating the stimulator of interferon genes (STING), TANK-binding kinase 1(TBK1), and interferon regulatory factor 3 (IRF3) pathway [9, 10]. It is currently unclear whether AIM2 and non-AIM2 DNA-sensing pathways interplay during RIAKI.

In the present study, we examined the roles of dsDNA and AIM2 in a mouse model of RIAKI in wild-type (WT) and *Aim2*−/− mice. Unexpectedly, *Aim2*-deficiency did not influence the severity of initial kidney injury, but did delay its recovery, and potentiated the subsequent inflammatory response and fibrosis. Loss of *Aim2* limited macrophage pyroptosis and instead accelerated

[1]Division of Inflammation Research, Center for Molecular Medicine, Jichi Medical University, Shimotsuke, Tochigi, Japan. [2]These authors contributed equally: Chintogtokh Baatarjav, Takanori Komada. ✉email: t_komada@jichi.ac.jp; masafumi2@jichi.ac.jp

Edited by M. Piacentini

Received: 12 November 2021 Revised: 9 June 2022 Accepted: 10 June 2022
Published online: 23 June 2022

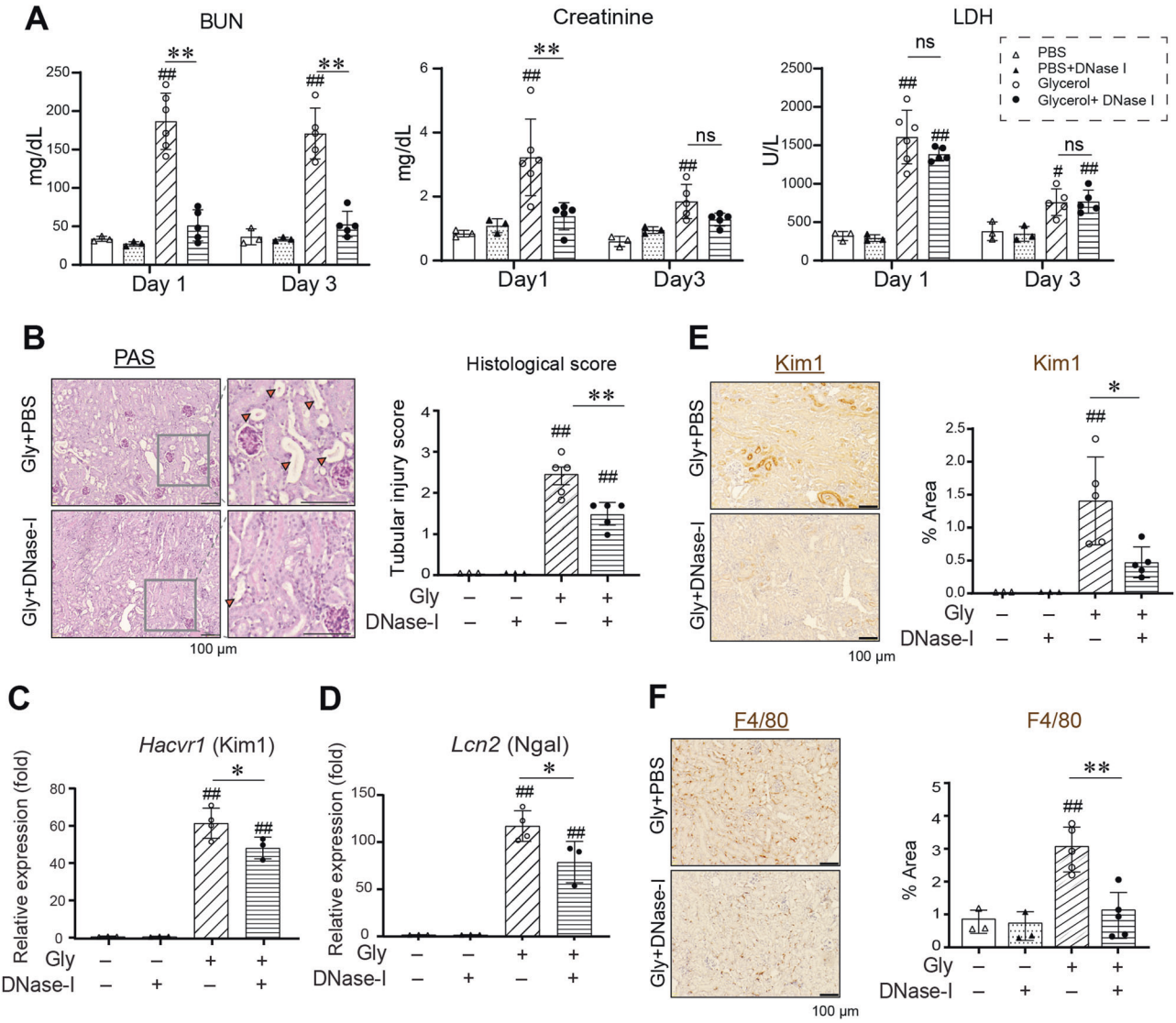

Fig. 1 dsDNA is a danger signal that triggers kidney epithelial injury and inflammation during RIAKI. DNase-I was administrated peritoneally just before and after glycerol injection and then every 12 h in WT mice. **A** Serum BUN, creatinine, and LDH levels at day 1 and day 3 ($n = 3, 3, 6, 5$ for Day 1, and 3, 3, 5, 5 for Day 3). **B** PAS staining of the kidneys at day 3 after glycerol injection. Orange arrowheads indicate tubular epithelial loss, tubular dilatation, and cast formation. Semi-quantitative assessment of tubular injury on PAS-stained sections ($n = 3, 3, 5$, and 5). **C**, **D** Kidney levels of *Kim1* and *Ngal* mRNA were analyzed by real-time RT-PCR ($n = 3, 3, 4$, and 3). **E** Immunohistochemistry for the Kim1-positive area was quantified ($n = 3, 3, 5$, and 5). **F** Immunohistochemistry for the F4/80-positive area was quantified ($n = 3, 3, 5$, and 5). Data are expressed as mean ± SD. $^{*}p < 0.05$ and $^{**}p < 0.01$; $^{\#}p < 0.05$ and $^{\#\#}p < 0.01$ vs. PBS with or without DNase-I.

subsequent inflammation by the recruitment of $CXCR3^{+}CD206^{+}$ macrophages during RIAKI. In in vitro experiments, dsDNA-treated *Aim2*-deficient macrophages engaged the STING-TBK1-IRF3/NF-κB pathway and released pro-inflammatory cytokines. Accordingly, the lack of prompt elimination of inflammatory macrophages by pyroptosis led to aberrant inflammation and impaired normal healing under *Aim2*-deficiency. Our results indicate that AIM2 pyroptosis is a critical mediator for the resolution of inflammation during RIAKI.

RESULTS

dsDNA is a danger signal that triggers kidney epithelial injury and inflammation during RIAKI

DNase-I is a potent endonuclease that hydrolyzes phosphodiester bonds and degrades extracellular double-stranded DNA (dsDNA) [11]. It reportedly mitigates the kidney dysfunction in RIAKI [4]. To verify the role of dsDNA as a DAMP during RIAKI, we first re-analyzed the effects of DNase-I in a mouse RIAKI model. Intramuscular glycerol injection elicited kidney dysfunction as characterized by increased serum BUN and creatinine levels, and DNase-I treatment significantly abrogated kidney dysfunction (Fig. 1A). This is not due to the effect of DNase-I on rhabdomyolysis, since LDH release was comparable between groups given vehicle or DNase-I. DNase-I treatment alleviated histological tubular epithelial injury, the upregulation of kidney injury molecule 1 (KIM1, or *Hacvr1*) and neutrophil gelatinase-associated lipocalin (Ngal, or *Lcn2*), and macrophage infiltration in the kidney after glycerol induction (Fig. 1B–F). These results indicate that extracellular dsDNA is an essential danger molecule that contributes to both kidney tubular epithelial damage and the accumulation of immune cells during RIAKI.

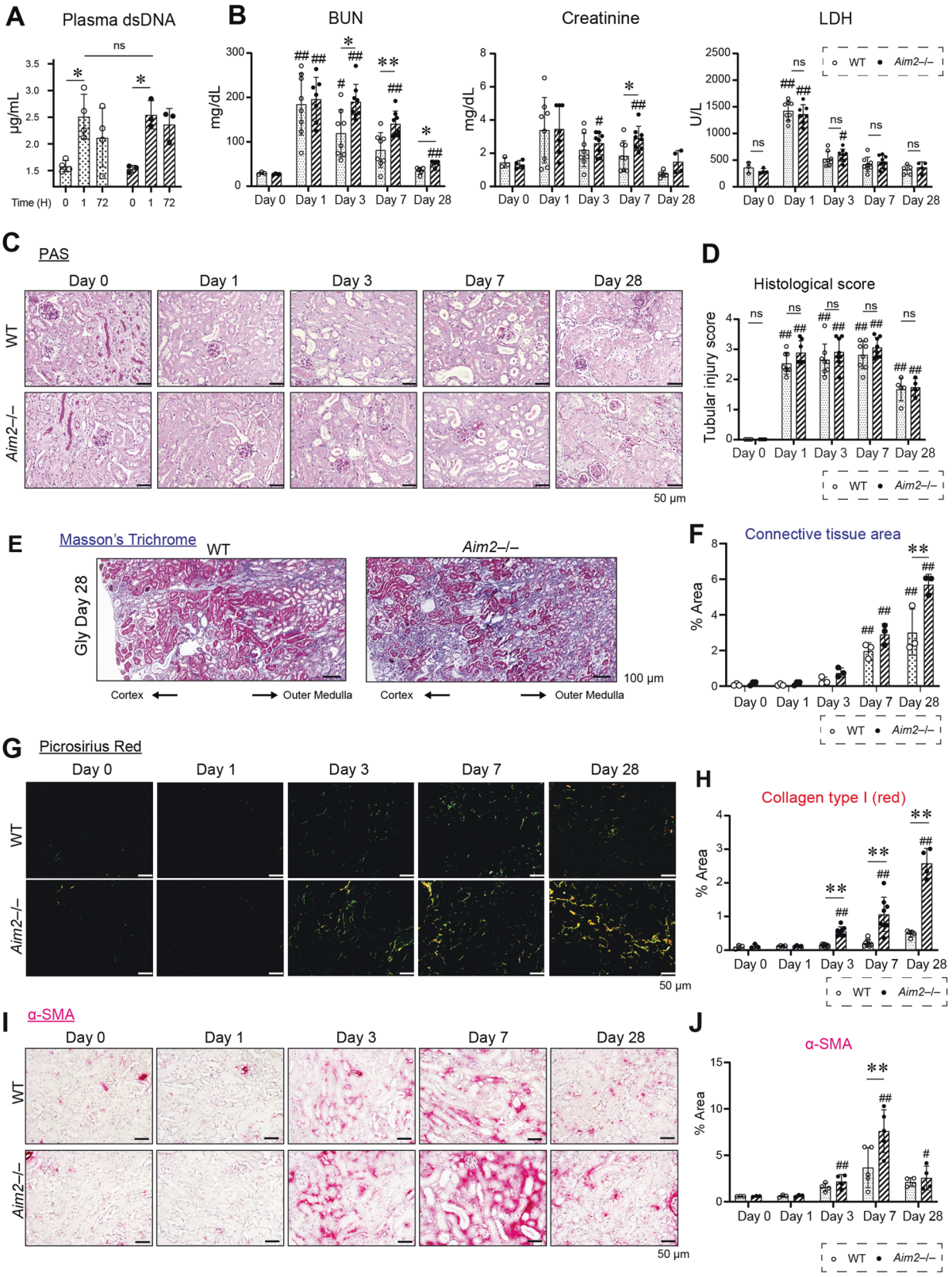

***Aim2*-deficiency delays functional recovery from RIAKI and promotes kidney fibrosis**

AIM2 is a cytosolic dsDNA sensor that is expressed in glomeruli, tubules, and immune cells of human and mouse kidneys [7, 12]. To examine whether AIM2 is involved in the pathogenesis of RIAKI, we aimed to investigate the phenotype of *Aim2*-deficient mice. Prior studies have suggested that *Aim2*-deficient congenic mice containing a 129/*SvJ* region display nonspecific immunophenotypic

Fig. 2 *Aim2*-deficiency delays functional recovery from RIAKI and promotes kidney fibrosis. A Plasma dsDNA was measured ($n = 4$ for WT mice, $n = 3$ for *Aim2*–/– mice) and (**B**) serum BUN, creatinine, and LDH levels ($n = 3$, 8, 8, 8, and 5 for WT, $n = 4$, 7, 8, 8, and 4 for *Aim2*–/–) were measured. **C**, **D** PAS staining of kidney samples from WT and *Aim2*–/– mice was used to assess kidney tubular injury. **C** Representative images are shown. **D** Semi-quantitative analysis of tubular injury ($n = 3$, 8, 8, 8, and 5 for WT, and $n = 4$, 7, 8, 8, and 4 for *Aim2*–/–). **E**, **F** Masson's Trichrome staining of the kidney samples from WT and *Aim2*–/– mice. **E** Representative images on day 28 are shown. **F** Connecting tissue area was quantified ($n = 3$ for each). Further representative images are shown in Supplementary Fig. 5. **G**, **H** Picrosirius red staining in the kidney cortex of WT and *Aim2*–/– mice was observed under polarized microscopy. **G** Representative images are shown. **H** Collagen type I (red) area was quantified ($n = 3$, 8, 8, 8, and 5 for WT, and $n = 4$, 7, 8, 8, and 4 for *Aim2*–/–). **I** Immunohistochemistry staining for αSMA (Days 0, 1, 3, 7, and 28) was performed. **J** The αSMA^+ area was quantified ($n = 3$, 3, 4, 5, and 4 for both WT and *Aim2*–/–). Data are expressed as mean ± SD. $^*p < 0.05$ and $^{**}p < 0.01$; $^{\#}p < 0.05$ and $^{\#\#}p < 0.01$ vs. day 0.

alterations by passenger mutations [13, 14]. To overcome this problem, we generated pure C57BL/6J-background *Aim2*–/– mice using a CRISPR/Cas9 knockout system (Supplementary Fig. 1). Analyses of isolated mouse bone marrow-derived macrophages (mBMDMs) validated *Aim2*-deficiency and its phenotypes (Supplementary Fig. 2). Indeed, dsDNA treatment introduced robust IL-1β release on lipopolysaccharide (LPS) -primed macrophages, and *Aim2*-deficiency efficiently abolished this response.

Experiments were conducted by analyzing the RIAKI model using these *Aim2*–/– mice. WT and *Aim2*–/– mice exhibited similar releases of dsDNA and LDH in circulation after glycerol administration (Fig. 2A, B), confirming that the loss of *Aim2* has no significant effect on the severity of rhabdomyolysis. According to the results of the DNase-I experiments, we initially expected the phenotypic amelioration in *Aim2*–/– against RIAKI. However, the peaks of the increase in serum BUN and creatinine levels were comparable at day 1 after RIAKI induction (Fig. 2B). Furthermore, *Aim2*-deficiency significantly delayed the recovery from kidney dysfunction, as demonstrated by a persistent increase in serum BUN and creatinine levels. Although isolated mouse tubular epithelial cells (mTECs) were susceptible to dsDNA, mTECs expressed a low level of Aim2 and were lacking in GSDMD (Supplementary Fig. 3). Tubular epithelia are unlikely associated with the phenotype of RIAKI, since tubular epithelial injury and proliferation did not differ between WT and *Aim2*–/– kidneys during the entire course (Fig. 2C, D, and Supplementary Fig. 4A–C).

Fibrosis is a hallmark of the transition of AKI to CKD [15, 16], and a single insult of RIAKI can also lead to irreversible scar formation in the kidney. During the recovery phase of RIAKI, kidneys displayed increased connective tissue and collagen deposition over time until 28 days after glycerol challenge (Fig. 2E–H and Supplementary Fig. 5). *Aim2*–/– kidneys showed more fibrotic area than WT. α-smooth muscle actin $(\alpha SMA)^+$ myofibroblast accumulation also developed, with a peak at day 7, and *Aim2*-deficiency promoted it more than WT at this time point (Fig. 2I, J). Together, these data show that *Aim2*-deficiency does not affect initial kidney tubular epithelial injury and retards kidney recovery from RIAKI, accelerating excessive fibrosis, indicative of the CKD transition.

$CXCR3^+CD206^+$ macrophages accumulate in *Aim2*-deficient kidneys during RIAKI

Large amounts of evidence have demonstrated that DAMP-associated sterile inflammation is a common cascade of AKI, and innate and adaptive immune responses participate in the development of fibrosis [17]. To assess the contribution of AIM2 to inflammation in RIAKI, we carried out an immunohistochemical analysis. Tubulointerstitial infiltration of $F4/80^+$ macrophages was clearly increased in RIAKI kidneys (Fig. 3A–C). *Aim2*–/– kidneys exhibited greater macrophage accumulation than WT. Macrophage infiltration in *Aim2*–/– RIAKI still depended on dsDNA since DNase-I alleviated this phenotype (Supplementary Fig. 4D, E). Notably, alternatively activated macrophages were more infiltrating in *Aim2*–/– kidneys, as demonstrated by upregulation of the mRNA for *Arg1* and *Cd206* at days 3–7 and immunostainings for Arginase-1 and CD206 (Fig. 3C–E). To characterize which type of macrophages were predominantly attracted during RIAKI, we evaluated mRNA levels of several chemokine receptors for monocytes/macrophages (Fig. 3F). Intriguingly, the kidney *Cxcr3* level was significantly higher in *Aim2*–/– kidneys. CXCR3 is known to be expressed by monocytes and macrophages, and $CXCR3^+$ macrophages can be attracted to the injured kidney [18]. It has been reported that $CXCR3^+$ macrophages partially exhibit alternatively activated phenotypes [19]. Accordingly, $CXCR3^+CD206^+$ macrophages were more accumulated in *Aim2*-deficient RIAKI kidneys (Fig. 3G). Hence, these results indicate that increased infiltration of alternatively activated macrophages in *Aim2*–/– RIAKI kidneys can attribute to CXCR3-mediated chemoattractant signalling.

Aim2-deficiency restricts macrophage pyroptosis and enhances NF-κB activation during RIAKI

In RIAKI, monocytes/macrophages are recruited to the injury site and contribute to disease progression and healing [20]. During a normal repair process, macrophages accumulate to engulf dead cells and remove debris. Concurrently, excessive or abnormally activated macrophages need to be eliminated to prevent their over-reaction to self-antigens [21]. To explore whether their cell death programs control macrophage numbers during RIAKI, we examined kidney tissues for macrophage cell death (Fig. 4A and Supplementary Fig. 6). Five days after RIAKI, dead macrophages ($CD45^+F4/80^+CD11b^+7\text{-}AAD^+$) were significantly increased in WT compared with *Aim2*–/– mice. Histological immunostaining also demonstrated $TUNEL^+F4/80^+$ macrophages in the WT kidneys of RIAKI, but these were scarce in *Aim2*–/– kidneys (Fig. 4B). Because neither 7-AAD nor TUNEL staining specifically detects pyroptosis, we assessed the inflammasome formation during RIAKI using ASC-Citrine reporter mice [22]. Citrine-aggregates, which suggested "ASC speck" formation, were observed in $F4/80^+$ macrophages in RIAKI kidneys (Fig. 4C). Furthermore, pyroptotic GSDMD cleavage was elicited during RIAKI in immunoblotting of total kidney lysate, and its cleavage was significantly diminished by *Aim2* deletion (Fig. 4D, E). Given the lack of GSDMD expression in isolated mTECs (Supplementary Fig. 3A), these results indicate that GSDMD-driven macrophage pyroptosis in the kidney occurs in WT mice, but not *Aim2*–/– mice, during RIAKI.

Along with this macrophage pyroptosis, we also analyzed inflammatory responses in RIAKI kidneys. Kidney expression of inflammasome-associated cytokines and IL-1β cleavage did not differ significantly between WT and *Aim2*–/– in the course of RIAKI (Supplementary Fig. 7). However, contrary to less macrophage pyroptosis, pro-inflammatory processes developed more in *Aim2*–/– kidneys after glycerol challenge, as demonstrated by the phosphorylation of nuclear factor-κB (NF-κB) p65 subunits (Fig. 4D, E) and higher levels of TNFα and interferon-β (IFNβ) proteins (Fig. 4F). TBK1 is an IKK-related serine/threonine kinase that mediates a non-canonical NF-κB activating cascade [23, 24]. Immunostaining for TBK1 phosphorylation displayed its cytoplasmic localization in $F4/80^+$ macrophages of *Aim2*-deficient RIAKI kidneys, significantly more than in WT RIAKI kidneys (Fig. 4G, H). These results suggest that TBK1/NF-κB and IFNβ signalling are involved in the mechanism of increased kidney inflammation under *Aim2*-deficiency.

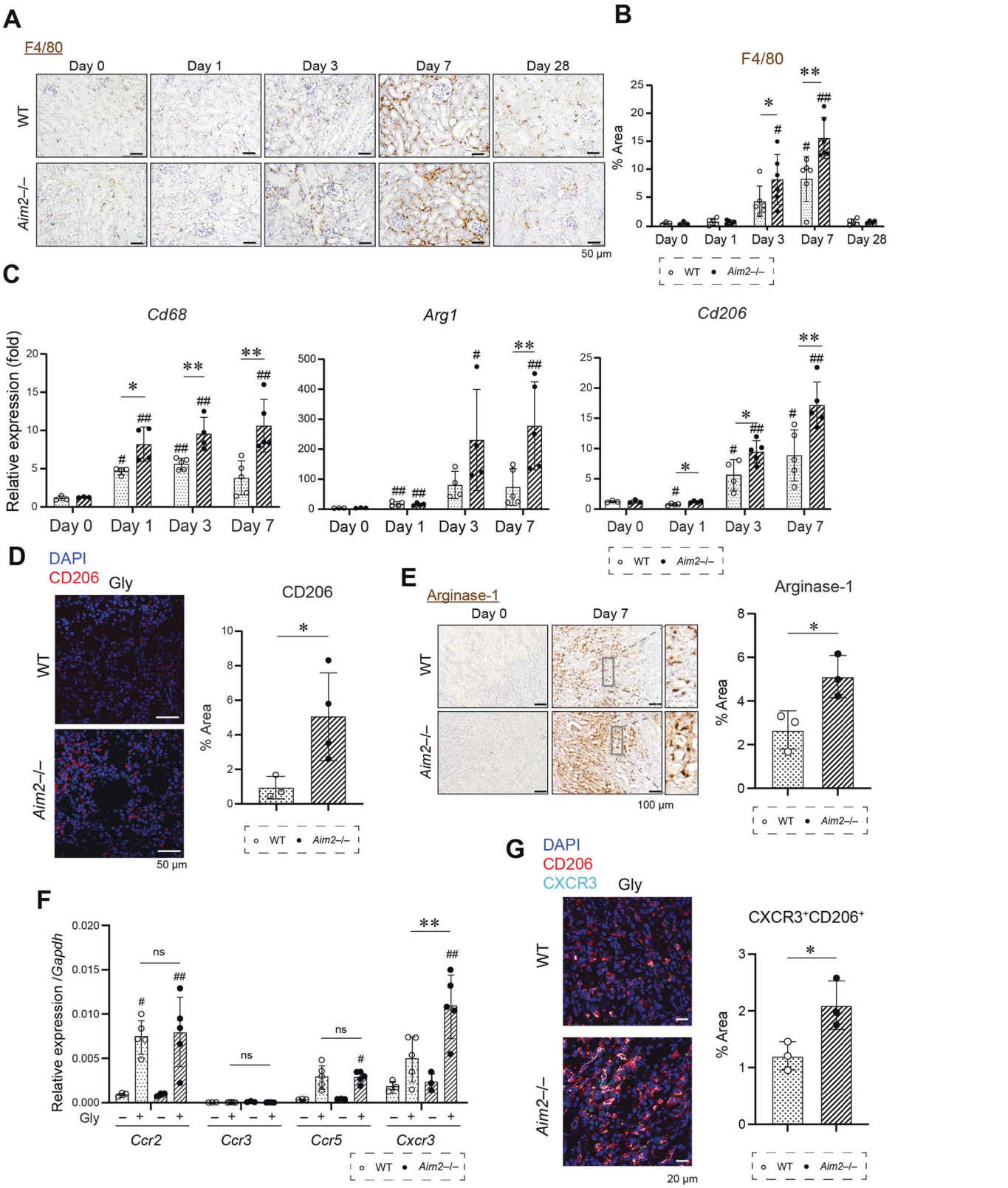

Swift AIM2 pyroptosis without IL-1β release is a feature of dsDNA-induced cell death in kidney macrophages

Pyroptosis is considered to be a highly pro-inflammatory death program since pyroptosis-driven cells potentially release IL-1β/IL-18 and other DAMPs [21]. Given this general notion, *Aim2*–/– RIAKI kidneys exhibited intriguing phenotypes. Macrophage pyroptosis was reduced. On the other hand, kidneys showed a greater pro-inflammatory response and macrophage accumulation, suggesting negative inflammatory regulation by AIM2 pyroptosis. To explain this discrepancy, we speculated that AIM2-dependent

Fig. 3 CXCR3$^+$CD206$^+$ macrophages accumulate in *Aim2*-deficient kidneys during RIAKI. A, **B** Immunohistochemistry for F4/80 was performed on kidney sections after RIAKI. **A** Representative images are shown. **B** Semi-quantitative assessment of F4/80$^+$ cells in the kidney ($n = 3$, 5, 6, 6, and 5 for WT, and $n = 3$, 5, 6, 6, and 4 for *Aim2*–/–; mean ± SD; *$p < 0.05$ and **$p < 0.01$. $^{\#}p < 0.05$ and $^{\#\#}p < 0.01$ vs. day 0). **C** The mRNA levels of macrophage markers *Cd68*, *Arg1*, and *Cd206* were analyzed by real-time RT-PCR in the RIAKI kidney ($n = 3$, 4, 5, and 5 for both WT and *Aim2*–/–; mean ± SD; *$p < 0.05$ and **$p < 0.01$. $^{\#}p < 0.05$ and $^{\#\#}p < 0.01$ vs. day 0). **D** Immunofluorescent staining for CD206 was performed on kidney sections 5 days after RIAKI. CD206$^+$ area in the kidney was quantified ($n = 3$ for WT, $n = 4$ for *Aim2*–/–; mean ± SD; *$p < 0.05$). **E** Immunohistochemistry staining for Arginase-1 was performed on kidney sections on days 0 and 7 after RIAKI. Arginase-1$^+$ area on day 7 was quantified ($n = 3$ for each; mean ± SD; *$p < 0.05$). **F** Leukocyte markers *Ccr2*, *Ccr3*, *Ccr5*, and *Cxcr3* in the kidneys 7 days after RIAKI were assessed by real-time RT-PCR ($n = 3$ and 5 mice for both WT and *Aim2*–/–; mean ± SD; *$p < 0.05$ and **$p < 0.01$. $^{\#}p < 0.05$ and $^{\#\#}p < 0.01$ vs. controls without glycerol injection). **G** Immunofluorescent staining for CXCR3 and CD206 was performed on the kidney sections 7 days after RIAKI. CXCR3$^+$CD206$^+$ area on day 7 was quantified ($n = 3$ for each; mean ± SD; *$p < 0.05$).

pyroptosis might eliminate macrophages before initiating pro-inflammatory signalling.

Under live-cell imaging and the LDH cytotoxicity assay, dsDNA caused immediate cell death within several hours in mBMDMs (Supplementary Movie, Fig. 5A, B). This necrotic cell death indisputably depended on AIM2, as *Aim2*-deficiency abrogated this rapid cell necrosis. Deficiency of other components of AIM2 pyroptosis, such as *Asc*, *Casp1/11*, or *Gsdmd*, abolished the GSDMD-cleavage in response to dsDNA treatment, and *Asc*–/– and *Casp1/11*–/– abrogated caspase-1 activation (Fig. 5C), which supports the engagement of AIM2 pyroptosis. Furthermore, dsDNA triggered similar immediate cell death on mouse kidney-resident macrophages (KRMs) isolated from glycerol-elicited RIAKI kidneys (geKRMs) (Supplementary Fig. 8A–C, Supplementary Movie). KRMs from untreated kidneys (naïve KRMs) and geKRMs exhibited caspase-1 activation and GSDMD cleavage after dsDNA treatment (Fig. 5D, E). These responses were strikingly suppressed in *Aim2*-deficient KRMs, suggesting that dsDNA-induced AIM2 pyroptosis is a common death program in macrophages of RIAKI kidneys irrespective of whether they are recruited or resident. Notably, neither pro-IL-1β nor mature IL-1β was detected in naïve/geKRMs regardless of dsDNA treatment or *Aim2* expression (Fig. 5F, G), revealing that dsDNA-induced AIM2 inflammasome activation drives pyroptosis without IL-1β release in KRMs.

These intriguing findings led us to examine whether pyroptosis without IL-1β release was a general feature of dsDNA-induced AIM2 inflammasome. dsDNA triggered pyroptotic cell death not only in classically activated macrophages, M(LPS/IFNγ), but also in unpolarized M(–) and alternatively activated M(IL-4) and M(TGFβ), as evidenced by LDH release and cleavage of caspase-1 and GSDMD (Fig. 5H, I, and Supplementary Fig. 8D–F). Interestingly, IL-1β expression and its maturation were only observed in short-time polarized M(LPS/IFNγ), and not in other macrophages, M(–), M(IL-4) and M(TGFβ). As shown above, IL-1β protein was also undetectable in naïve/geKRMs (Fig. 5F, G). These results demonstrate that macrophages in the kidney operate AIM2 pyroptosis triggered by dsDNA regardless of their origin or polarization. Pro-inflammatory IL-1β release by dsDNA-induced AIM2 pyroptosis is exclusively context-dependent and probably requires prerequisite priming stimuli, which explains the less-inflammatory phenotypes of *Aim2*-intact kidneys.

Aim2-deficient macrophages drive STING signalling by sensing dsDNA

In the absence of AIM2, cytosolically-misplaced dsDNA can alternatively engage other DNA sensors. Most dsDNA sensors, such as cGAS, DAI, IFI16, DDX41, and DNA-protein kinase (DNA-PK), mediate the STING-TBK1-IRF3 pathway leading to pro-inflammatory responses [25]. To examine the potential STING activation in *Aim2*–/– macrophages, we performed immunostaining for phosphorylated TBK1 in geKRMs and bone marrow-derived M(–) macrophages (Fig. 6A, B). *Aim2*-deficient geKRMs and mBMDMs clearly developed TBK1 phosphorylation in response to dsDNA; in contrast, WT cells responded with no or little phosphorylation. We next analyzed immunoblotting for TBK1/IRF3 signalling and NF-κB activation after dsDNA treatment. As previously reported [26], *Aim2*-deficient M(–) macrophages potentiated the phosphorylation of these proteins (Fig. 6C). dsDNA-treated *Aim2*-deficient macrophages also displayed band shifts of STING protein as a result of its activation (Fig. 6C) [27, 28]. geKRMs exhibited a similar response in phosphorylation, although WT geKRMs expressed more total protein levels of Sting, TBK1, IRF3 and p65, probably due to a skewed polarization in geKRMs (Supplementary Fig. 9A, B). In any case, the polarization of mBMDMs did not interfere with this STING-TBK1-IRF3/NF-κB phosphorylation cascade under *Aim2*-deficiency (Supplementary Fig. 9C, D). In contrast, mTECs did not alter this pathway by *Aim2* expression (Supplementary Fig. 9E), which demonstrates the cell-type specificity of AIM2 functions.

When M(–) macrophages were treated with dsDNA, downstream genes of the STING pathway including C-X-C motif chemokine (CXCL) 10 (CXCL10), TNFα, and IFNβ were upregulated in a dose-dependent manner and further augmented in *Aim2*–/– macrophages, compared to WT macrophages (Supplementary Fig. 10A). In an analysis of the supernatant, TNFα and IFNβ were vigorously secreted by dsDNA treatment in *Aim2*-deficient geKRMs/M(–) (Fig. 6D, E, and Supplementary Fig. 10B). Inhibition of protein synthesis by cycloheximide abolished dsDNA-induced cytokine secretion in both WT and *Aim2*-deficient macrophages (Fig. 6F), which supports the notion that dsDNA evokes *de novo* cytokine production in surviving cells. Furthermore, this cytokine secretion was efficiently suppressed by a STING inhibitor, H151 [29], which supports their STING-mediated responses (Fig. 6G). On the other hand, the DNA-PK inhibitor Nu-7441 did not reduce TNFα secretion in *Aim2*–/–, indicating that it makes only a limited contribution to the STING pathway (Supplementary Fig. 10C). Taken together, these findings suggest that *Aim2*-deficient macrophages activate the STING-TBK1-IRF3/NF-κB pathway in response to dsDNA, leading to pro-inflammatory cytokine maturation and secretion, which explains the more inflammatory phenotypes of *Aim2*–/– kidneys.

Escape from AIM2 pyroptosis propagates inflammation to surrounding cells

Experiments were performed to evaluate the response of neighbouring cells to dsDNA-treated macrophages. We incubated mBMDMs and mTECs with conditioned medium derived from WT or *Aim2*-deficient geKRMs or mBMDMs with dsDNA treatment (Fig. 7A). After incubation with conditioned medium of dsDNA-treated *Aim2*-deficient geKRMs, acceptor mBMDMs displayed the upregulation of pro-inflammatory genes, such as *Ccl2* and *Il1b* whereas acceptor mTECs showed a minor response (Fig. 7B, C). Conditioned medium from *Aim2*–/– mBMDMs similarly boosted these gene expressions (Fig. 7D). We speculated that Sting-mediated cytokines in *Aim2*–/– conditioned medium contributed, rather than inflammasome-associated cytokines and DAMPs. dsDNA-treated geKRMs/M(–) gave off little IL-1 and no different

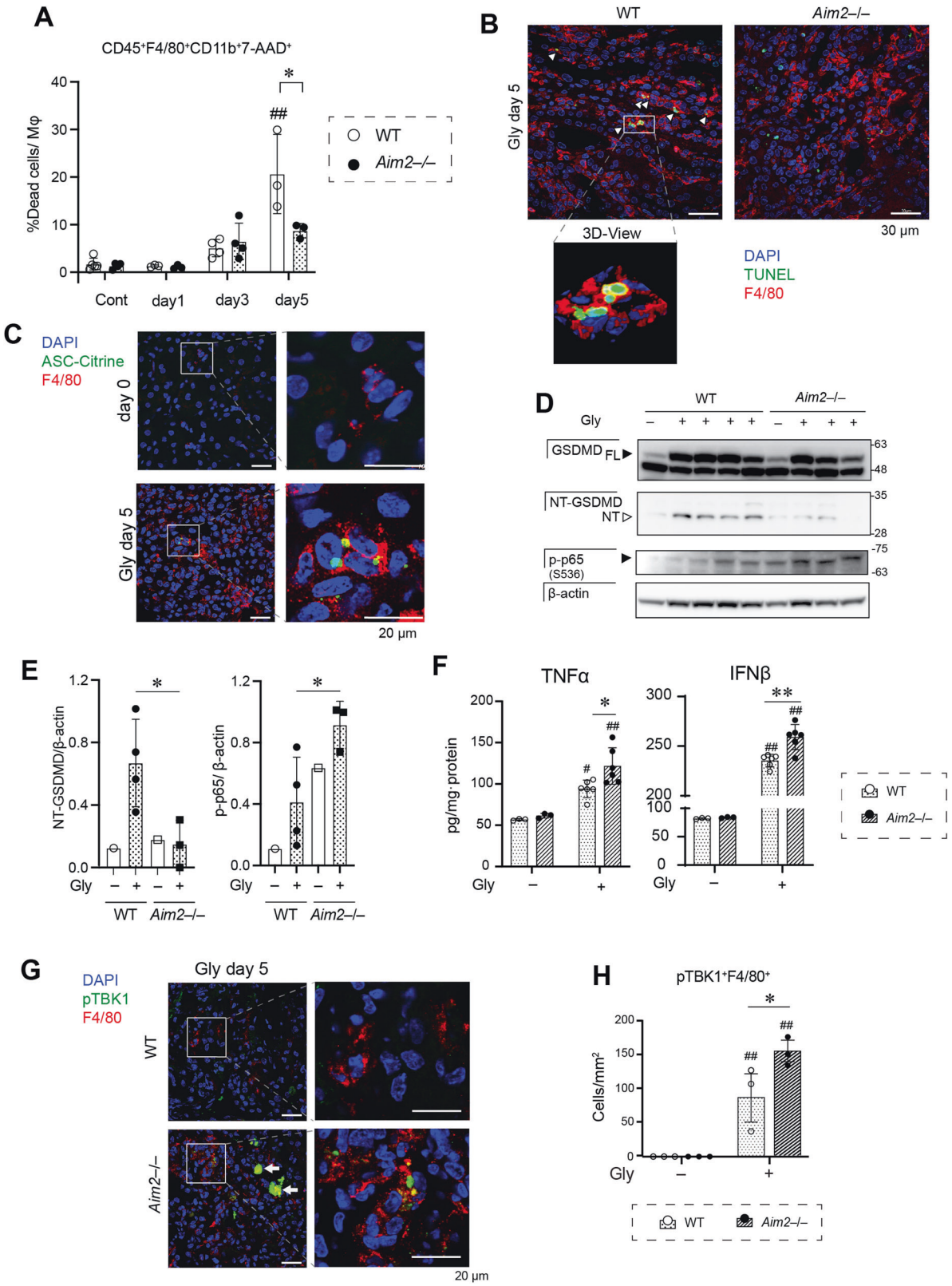

amount of high mobility group box 1 (HMGB1) between WT and *Aim2*–/– (Supplementary Fig. 11). Indeed, the increased pro-inflammatory cytokine levels by conditioned medium were effectively blunted when Sting signalling was blocked by H151 in donor mBMDMs (Fig. 7D). These results reveal that Sting-dependent humoral factors from *Aim2*-deficient survivor cells propagate inflammatory responses to neighbouring cells, especially to macrophages.

Fig. 4 *Aim2*-deficiency restricts macrophage pyroptosis and enhances NF-κB activation during RIAKI. A Flow cytometric analysis for detecting $CD45^+F4/80^+CD11b^+7\text{-}AAD^+$ cells in WT and *Aim2*–/– mice after glycerol injection ($n = 4$, 3, 4, and 3 for both WT and *Aim2*–/–; mean ± SD; $^*p < 0.05$). **B** Immunofluorescent staining for F4/80 (red) and TUNEL (green) in WT and *Aim2*–/– kidneys 5 days after RIAKI. White arrowheads indicate $TUNEL^+F4/80^+$ macrophages. **C** Immunofluorescent staining for F4/80 (red) in ASC-Citrine mice 5 days after glycerol injection. ASC-Citrine aggregates are shown in green. **D** Kidney expression of GSDMD, cleaved amino-terminal (NT)-GSDMD and phosphorylated NF-κB p65 subunit (p-p65; Serine 536) was assessed by immunoblotting. **E** Semi-quantitative analysis of immunoblotting for NT-GSDMD and p-p65 was performed. β-actin was used as the internal control ($n = 1$ and 4 for WT, and 1 and 3 for *Aim2*–/–; mean ± SD; $^*p < 0.05$). **F** Total protein lysates were prepared from the kidney 5 days after glycerol treatment using RIPA lysis buffer with protease inhibitors. Kidney TNFα and IFNβ were measured using ELISA ($n = 3$, 3, 6, and 6; mean ± SD; $^*p < 0.05$ and $^{**}p < 0.01$; $^{\#}p < 0.05$ and $^{\#\#}p < 0.01$ vs. controls without glycerol injection). **G** Immunofluorescent staining for pTBK1 and F4/80 was performed on the kidney sections 5 days after RIAKI. White arrows indicate debris with nonspecific fluorescence. **H** $pTBK1^+F4/80^+$ cells were quantified ($n = 3$ for each; mean ± SD; $^*p < 0.05$ and $^{**}p < 0.01$; $^{\#\#}p < 0.01$ vs. controls without glycerol injection).

DISCUSSION

In the current study, we elucidated the mechanisms of increased kidney inflammation during RIAKI in the context of *Aim2*-deficiency. Although *Aim2*-deficient macrophages do not operate dsDNA-induced pyroptosis, these surviving macrophages drive alternate DNA-sensing pathways resulting in excessive inflammation and fibrosis (Fig. 8). dsDNA engenders pyroptotic cell death in diverse macrophages without processing of pro-IL-1β. *Aim2*-deficient macrophages lacking pyroptotic machinery rather propagate an inflammatory response to their surroundings via STING-mediated cytokines, possibly contributing to macrophage attraction and the activation status. Our findings clearly demonstrate an unexpected role of AIM2 pyroptosis in limiting inflammation.

Nucleic acids are widely accepted as pathogen-associated molecular patterns (PAMPs) or DAMPs and are associated with ageing and various disease pathologies (e.g., Aicardi-Goutiéres syndrome, systemic lupus erythematosus, cancer, cystic fibrosis, and Alzheimer's disease). Although its precise sources are still uncertain, we identified extracellular dsDNA as a critical DAMP of RIAKI (Fig. 1). Many cytosolic DNA sensors have been identified to date, such as AIM2, cGAS, DAI, IFI16, DDX41, and DNA-PK [25]. AIM2 is a well-known PRR that assembles inflammasomes directly upon binding to dsDNA. In the kidney, AIM2 is constitutively expressed in glomerular podocytes, tubular epithelial cells, and leukocytes [7, 12]. Leukocytes such as macrophages and dendritic cells have a capacity for inflammasome assembly. In the pathogenesis of CKD, the AIM2 inflammasome plays a critical role mediated through interaction between necrotic cell death and inflammation [7]. Akin to CKD, we expected that macrophages during RIAKI take up necrotic DNA in an AIM2-dependent manner. In our study, macrophages operate AIM2 pyroptosis in RIAKI based on evidence of macrophage ASC speck formation and cleavage of GSDMD (Fig. 4). Our results strongly support the notion that AIM2 pyroptosis occurs in macrophages during RIAKI.

Cell death is a physiologically functional process that conveys signals to the cell surroundings. Pyroptosis, which is defined as a type of regulatory cell death induced by the plasma membrane pores of gasdermin proteins [30], has been considered to be highly pro-inflammatory because DAMPs such as high mobility group box 1 (HMGB1) and cytokines can be released during cell lysis [31]. IL-1 cytokines given off by classically activated macrophages contribute to its pro-inflammatory outcomes. However, IL-1 cytokines seemed to play a minor role in the excessive inflammation of *Aim2*-deficient RIAKI kidneys (Supplementary Fig. 7). We instead demonstrated a surprising function of AIM2 pyroptosis in limiting inflammation by rapidly halting cell functions. Indeed, the AIM2 inflammasome and GSDMD-induced cell death during development reportedly regulate neuronal homeostasis without processing of IL-1 [32]. It is likely that rapid macrophage degradation terminates viable cell functions and restricts further cytokine production. Given our results that cycloheximide effectively limits cytokine release (Fig. 6F), cells require sufficient time for STING-mediated transcriptional/translational processes to obtain a pro-inflammatory phenotype. In line with our observation, previous studies have demonstrated that pathogens enhance the type I IFN response due to cGAS/STING activation in the absence of AIM2 in macrophages/dendritic cells [26, 33]. Our animal experiments identified the further expansion of $CXCR3^+CD206^+$ macrophages in the tubulointerstitial area in *Aim2*-deficient RIAKI kidneys (Fig. 3), which is probably mediated through the STING/CXCL10/CXCR3 axis. Our study clearly demonstrates that rapid AIM2 pyroptosis prevents the pro-inflammatory STING axis in vitro and in vivo.

Mechanistically, direct interactions between the AIM2 inflammasome and the STING pathway have been proposed by other groups: for example, the CARD domain of ASC can bind to the N-terminal domain or the CTT domain of STING to regulate TBK1 activation [33]; canonical caspase-1 or non-canonical caspase-4/-5/-11 directly cleave cGAS and inactivate downstream STING/type I IFN signalling [34, 35]. It has also been reported that K^+ efflux through inflammasome-mediated GSDMD pores restricts cGAS/STING signalling [36]. Furthermore, inflammasome-independent functions of AIM2 may be involved. Mouse homologues Ifi202, Ifi204, and Ifi205 activate the STING-mediated type I IFN pathway, and AIM2 can antagonize this signalling [14, 37, 38]. As recently reported, AIM2 negatively regulates the DNA-PK/AKT3/IRF3 pathway and limits neuroinflammation in microglia [39]. Although the interaction of AIM2 with DNA-PK can be critical, DNA-PK seemed to make only a limited contribution to type I IFN activation of *Aim2*-deficient macrophages in our experiments (Supplementary Fig. 10C). How AIM2 has priority over other DNA sensors still needs to be elucidated. The complex interplay among these DNA-sensing pathways is a challenge for future studies.

Although we identified that inflammasomes and pyroptosis are crucial in RIAKI, the role of each component is also perplexed. First, the dsDNA-induced pyroptosis seems to possess backup machinery. Prior studies have shown that apoptosis and gasdermin E (GSDME)-dependent secondary necrosis are driven by macrophages lacking in GSDMD or caspase-1 [40, 41]. In our hands, *Gsdmd*–/– mice did not display aggravation in RIAKI, including tubular injury and macrophage accumulation (Supplementary Fig. 12). We speculate that rapid apoptotic macrophage death might substitute for pyroptotic elimination. Supporting this, activation of caspase-3/GSDME was prominent in macrophages derived from *Gsdmd*-deficient RIAKI kidneys (Supplementary Fig. 13). Second, activation of NLRP3 and AIM2 in RIAKI is deemed cell-/site-specific and has different roles. Our previous work has demonstrated that *Nlrp3*–/– mice exhibited less tubular damage during RIAKI as well as *Asc*–/–, *Casp1*–/–, and *IL1b*–/– mice [8]. It is noteworthy that tubular damage occurs before leukocyte accumulation, suggesting that NLRP3 inflammasome components and IL-1β directly impact tubular apoptosis. Indeed, NLRP3 and ASC in tubules participate in tubular apoptosis [42, 43]. Furthermore, collecting ducts (CD) express NLRP3 inflammasome components and IL-1β, and may function in this segment [44, 45]. Although how inflammasomes in CD potentiate tubular injury during RIAKI is still uncertain, less tubular injury in *Casp1*–/– and *Il1b*–/– RIAKI might be due to the inoperative NLRP3

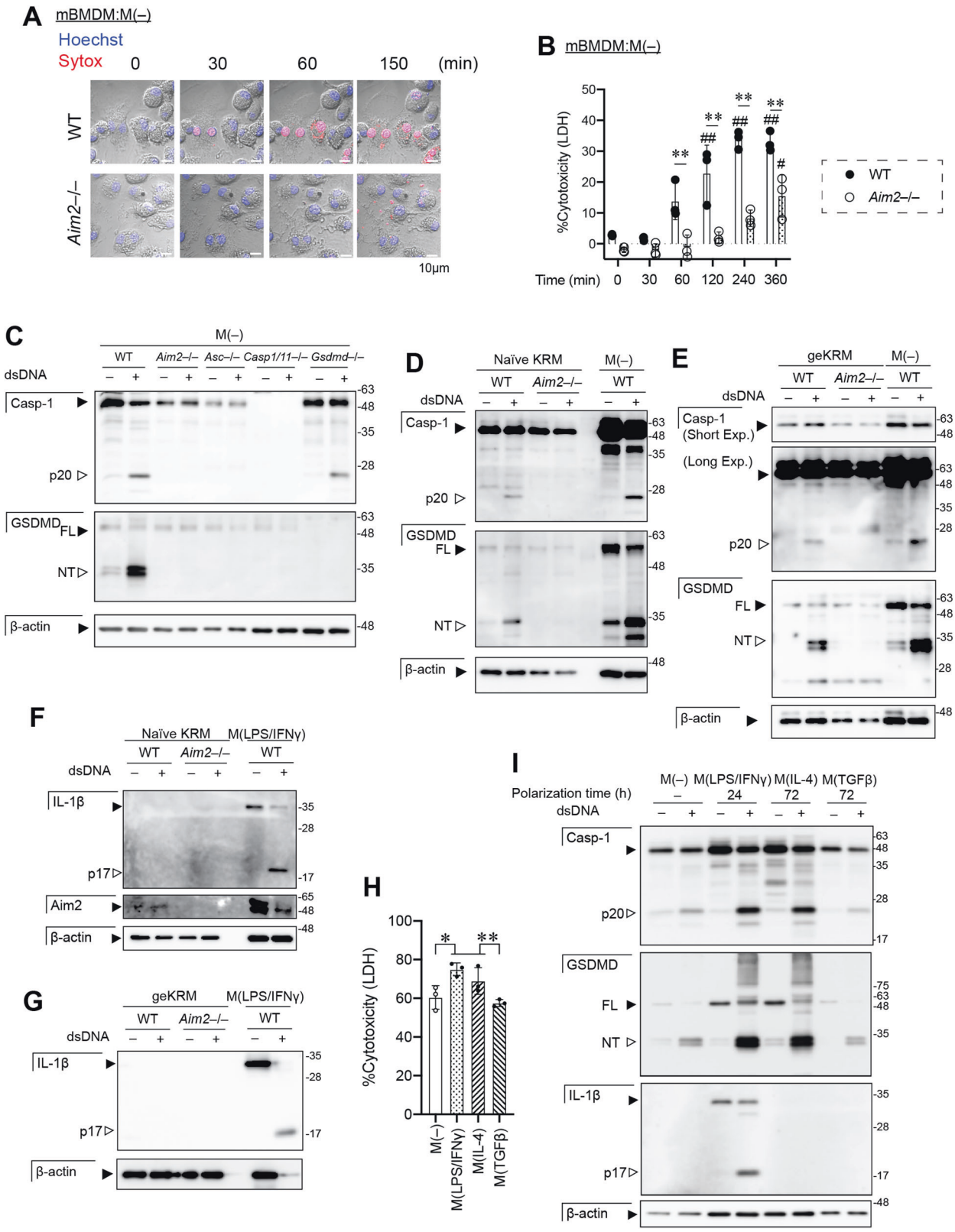

inflammasome pathway in CD [8]. By contrast, the deletion in *Aim2* and *Gsdmd* did not affect tubular injury and IL-1β processing (Supplementary Fig. 7B–D, 12E, F), suggesting that AIM2 pyroptosis occurs in cells distinct from IL-1β processing sites. The expression sites and roles of AIM2 in the kidney are different from NLRP3. For example, AIM2 in glomerular podocytes has an inflammasome-independent role in suppressing inflammation and cell proliferation during glomerulonephritis [12]. Inflammasome-independent functions of AIM2 and kidney cell-specific properties of AIM2 inflammasome remain to be investigated.

Fig. 5 Swift AIM2 pyroptosis without IL-1β release is a feature of dsDNA-induced cell death in kidney macrophages. A mBMDMs derived from WT and *Aim2*–/– mice were observed under time-lapse live-cell imaging for 2.5 h. Nuclei were stained with Hoechst 33342 (blue), and cell-impermeable Sytox dye (Red) detected dead cell nuclei. After cells were treated with dsDNA, images were obtained every 10 min and are shown as brightfield, Hoechst, and Sytox overlays. **B** Cytotoxicity of dsDNA was assessed by LDH release in supernatant ($n = 3$ for each group, mean ± SD; $^{**}p < 0.01$. $^{\#}p < 0.05$ and $^{\#\#}p < 0.01$ vs. controls at time zero). **C** Unpolarized mBMDMs (M(–)) were isolated from WT, *Aim2*–/–, *Asc*–/–, *Casp1/11*–/–, and *Gsdmd*–/– mice. Immunoblotting for caspase-1, GSDMD, and β-actin was performed using a total cell/supernatant mixture 6 h after dsDNA treatment. **D**–**G** Mouse kidney resident macrophages (KRMs) isolated from healthy kidneys (naïve KRMs) or glycerol-elicited RIAKI kidneys (geKRMs) were isolated using a magnetic bead isolation method. **D**, **E** Immunoblotting of naïve/geKRMs for caspase-1, GSDMD, and β-actin was performed 6 h after dsDNA treatment. **F**, **G** Immunoblotting of naïve/geKRMs for IL-1β, Aim2, and β-actin. **H** LDH cytotoxicity assay on mBMDMs after polarization: M(–), unpolarized; M(LPS/IFNγ), M(IL-4), and M(TGFβ) ($n = 3$ for each; mean ± SD; $^{*}p < 0.05$ and $^{**}p < 0.01$). **I** Immunoblotting of polarized mBMDMs for caspase-1, GSDMD, IL-1β, and β-actin was performed 6 h after dsDNA treatment.

In conclusion, we found that STING-mediated inflammation is accelerated during RIAKI under the lack of AIM2 pyroptosis machinery. Our results provide evidence that dsDNA-induced AIM2 pyroptosis is critical in limiting kidney inflammation after a sudden strike of rhabdomyolysis. Endogenous extracellular dsDNA works as a DAMP on kidney cells and macrophages in the pathogenesis of RIAKI and subsequently contributes to the progression of AKI to CKD. The DNase-I treatment alleviated dsDNA-mediated immunopathology in RIAKI regardless of whether AIM2 exists (Fig. 1, Supplementary Fig. 4D, E), which indicates that DNase-I is also effective in AIM2-independent pathways. Further dissecting the signalling of dsDNA sensors and targeting these specific pathways would mitigate the progression of the continuum of AKI to CKD.

METHODS (SUBJECTS) AND MATERIALS

Mouse studies and a mouse RIAKI model

C57BL6/J wild-type (WT) mice were purchased from SLC Inc. (Shizuoka, Japan). *Aim2*–/– mice on a background of C57BL/6J were generated by CRISPR/Cas9-based genome editing at the Laboratory Animal Resource Center, University of Tsukuba (Tsukuba, Japan). Genome editing in fertilized mouse eggs was performed using methods reported previously [46]. Exon 6 of the WT murine *Aim2* allele (Genebank NC_000067.6) was targeted for CRISPR/Cas9 deletion (Supplementary Fig. 1A). *Aim2*–/– mice developed normally and were genotyped with PCR primers of 5′-TGGAGTTCAGGCAGATTCGG-3′and 5′-ATGTGGCACTCCGGTAGTATG-3′ for a 310-bp WT DNA product, and 5′-TGGAGTTCAGGCAGATTCGG-3′and 5′-GTATGTGTGTTTGCCCACGC-3′ for a 720-bp mutant DNA product (Supplementary Fig. 1B). Inflammasome-activating phenotypes were validated with isolated mBMDMs by treatment with LPS and poly (dA;dT) transfection (Supplementary Fig. 2). *Asc*–/–, and *Casp1/11*–/– mice were provided by Drs. Shun'ichiro Taniguchi (Shinshu University, Matsumoto, Japan) and Hiroko Tsutsui (Hyogo College of Medicine, Nishinomiya, Japan), respectively [47–49]. *Gsdmd*–/– mice were developed by Genentech [50] and provided by Dr. Kate Schroder (The University of Queensland, Brisbane, Australia). ASC-Citrine (B6.Cg-*Gt(ROSA)26Sor*$^{tm1.1(CAG-Pycard/mCitrine*,-CD2*)Dtg}$/J) mice [22] were obtained from The Jackson Laboratory (Bar Harbor, ME, United States). All mice were maintained under a 12-h light/dark cycle, with food and water provided ad libitum. Female mice aged 8–12 weeks were used for cell experiments. Male mice aged 8–10 weeks from vendor's colonies of WT, and in-house colonies of *Aim2*–/– and *Gsdmd*–/– were used for a murine RIAKI model. RIAKI was produced by intramuscular injection into both hind limbs with 50% glycerol (5 mL/kg) or vehicle (0.9% saline) as a control, after water deprivation for 24 h [8, 51]. DNase-I (Sigma-Aldrich, St. Louis, MO, USA) was injected intraperitoneally (50 KU) every 12 h after the initial two doses: immediately before (10 KU) and after (50 KU) glycerol injection. Control mice were injected with vehicle (PBS with 0.15 mg/mL $CaCl_2$). Mice were sacrificed at the indicated time points following glycerol injection. Mice were randomly assigned to groups in experiments, but no blinding was performed during animal experiments and the isolation of primary cells.

Cell culture

mBMDMs were isolated from femurs and tibias, and cultured in RPMI-1640 (Wako, Osaka, Japan) supplemented with 10% fetal bovine serum (FBS), 1% Antibiotic Antimycotic Solution (Sigma, St. Louis, MO, USA) and 15% conditioned medium of L929 cells (ATCC, Rockville, MD, USA) for 7 days. BMDMs were further cultured for 24 h in the above-mentioned medium containing 100 nM LPS (L4391, Sigma) and 10 ng/mL interferon γ (IFNγ) (315-05, PeproTech, Cranbury, NJ, USA) for classically activated macrophage M(LPS/IFNγ) polarization. Media containing 20 ng/mL IL-4 (214-14, PeproTech), 10 ng/mL TGFβ (100-21 C, PeproTech) were used for 72-hour polarization of alternatively activated macrophages M(IL-4) and M(TGFβ). For the activation of AIM2 or other dsDNA sensors, cells were transfected with poly (dA:dT) (InvivoGen, San Diego, CA, USA) using Lipofectamine 2000 (Thermo Fisher Scientific, Waltham, MA, USA) according to the manufacturer's protocol. Cells were not primed unless stated otherwise.

Primary mTECs were isolated from mice as previously reported [7, 52]. After mice were sacrificed, kidneys were immediately removed. Kidney cortexes were minced and incubated in RPMI 1640 containing 1 mg/mL collagenase P (Sigma) at 37 °C for an hour. Cells were passed through a 70-μm cell strainer, washed with PBS (–) twice and plated on dishes. mTECs were grown in DMEM/F-12 medium with 10% FBS, 125 ng/mL prostaglandin E1, 25 ng/mL EGF, 1.8 μg/mL L-thyroxine, 3.38 ng/mL hydrocortisone, and 2.5 mg/mL insulin-transferrin-sodium selenite mix. Cells were grown at 37 °C in a 5% CO_2 atmosphere. Cells were used within two passages. For the AIM2 activation assay, cells were transfected with poly (dA:dT) using Lipofectamine 2000 and incubated for 24 h.

Primary naïve KRMs were isolated from healthy male WT and *Aim2*–/– mice aged 8–12 weeks. Glycerol-elicited (ge) KRMs were isolated from mice that underwent intramuscular injection of 50% glycerol (5 mL/Kg) 5 days before. After perfusion with 10 mL saline from the heart, kidneys were harvested, minced, and digested in collagenase P-containing media for an hour at 37 °C. After incubation in ACK buffer for 8 min on ice, cells were resuspended in 40% Percoll (GE Healthcare) and layered on 80% Percoll followed by centrifugation at 500 x g for 30 min. Leukocytes at the interface were isolated, washed, and resuspended in PBS(–). $CD11b^{+}$ monocytes/macrophages were further purified by using mouse/human CD11b MACS MicroBeads (130-049-601, Miltenyi Biotec, Bergisch Gladbach, Germany) according to the manufacturer's protocol. KRMs were grown in RPMI-1640 containing 10 ng/mL M-CSF (315-02, PeproTech) for 2 days. For the activation of AIM2 or other dsDNA sensors, cells were transfected with poly (dA:dT) using Lipofectamine 2000 according to the manufacturer's protocol. Cells were not primed unless stated otherwise.

Real-time RT-PCR

Total RNA was isolated from the whole kidney or cultured cells using ISOGEN (Nippon Gene, Toyama, Japan) according to the

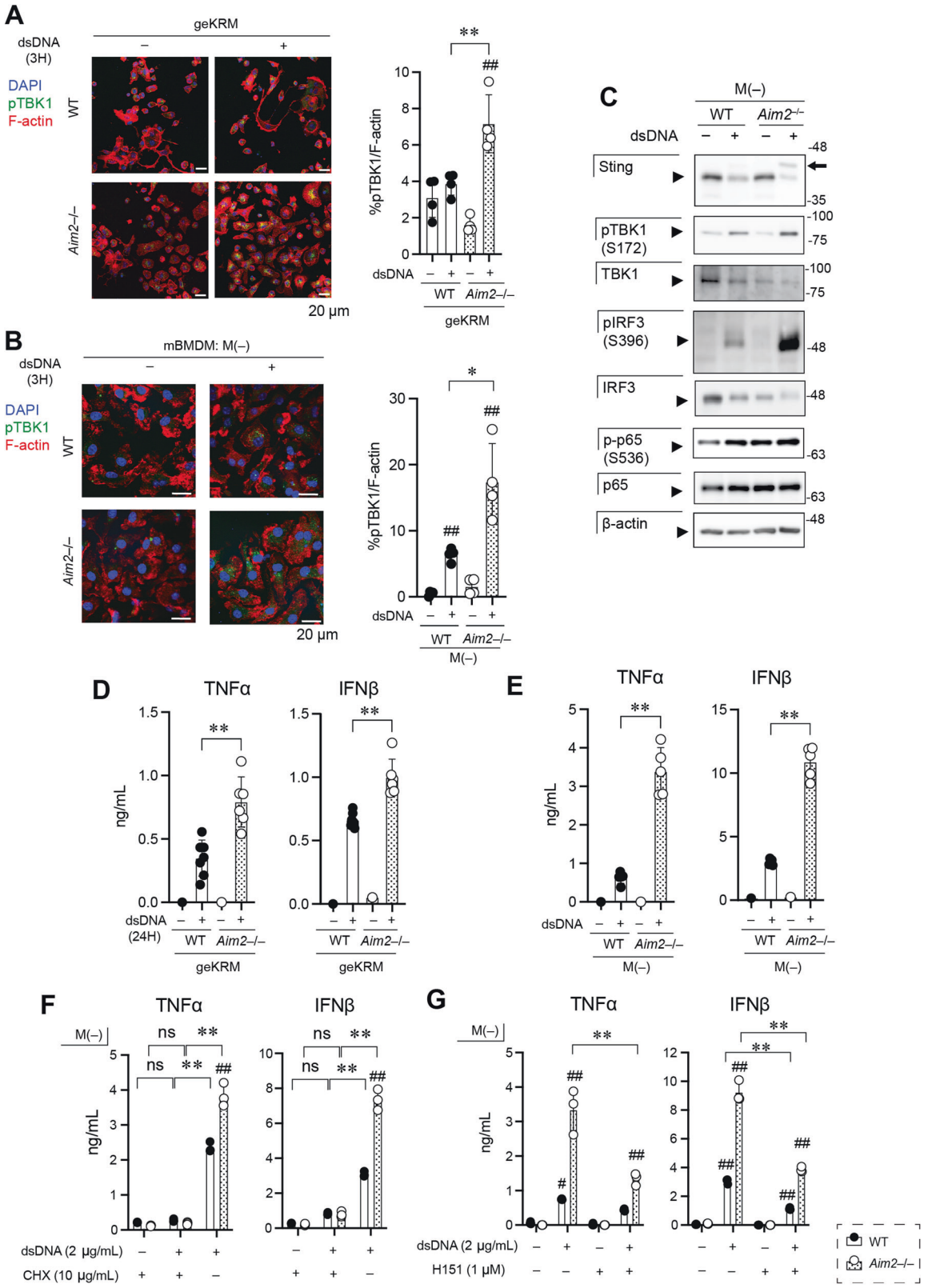

manufacturer's instructions. The following primers were used: *Actb* (Forward, 5′-CACAGCTTCTTTGCAGCTCCTT-3′, reverse, 5′-AGCGCAGCGATATCGTCAT-3′), *Arg1* (Forward, 5′-ACAAGACAGGGCTCCTTTCA-3′, reverse, 5′-AGCAAGCCAAGGTTAAAGCC-3′), *Ccl2* (Forward, 5′-GGCTCAGCCAGATGCAGTTAAC-3′, reverse, 5′-GCCTACTCATTGGGATCATCTTG-3′), *Ccr2* (Forward, 5′-CCTGCAAAGACCAGAAGAGGG-3′, reverse, 5′-GAGATGTTGATAGTATGCCGTGGA-3′), *Ccr3* (Forward, 5′-TGGCAATTTCTGACCTGCTCT-3′, reverse, 5′-AACCCAGACAGCATTTTGCAC-3′), *Ccr5* (Forward, 5′-CTGGCAAAAAGCTGAAGAGCGT-3′, reverse, 5′-GCAGCATAGTGAGCCCAGAAT-3′), *Cd206*

Fig. 6 *Aim2*-deficient macrophages drive STING signalling by sensing dsDNA. A, **B** geKRMs and unpolarized mBMDMs (M(–)) were treated with or without 2 μg/mL poly (dA:dT) for 3 h. Immunofluorescent staining was performed for phosphorylated TBK1 (pTBK1, green). Representative images are shown. DAPI (Blue) and Phalloidin (Red) were reacted for staining nuclei and F-actin, respectively. Quantification of $pTBK1^+$ cell numbers were performed ($n = 4$ for each; mean ± SD; $^*p < 0.05$ and $^{**}p < 0.01$, $^{\#\#}p < 0.01$ vs. controls without dsDNA). **C** Immunoblotting analysis of Sting, phosphorylated TBK1 (Serine 172), TBK1, phosphorylated IRF3 (Serine 396), IRF3, p-p65 (Serine 536), total p65, and β-actin was performed on M(–). Arrows indicate shifted bands of Sting. **D**, **E** geKRMs and M(–) were treated with indicated concentrations of dsDNA for 24 h. Cytokine release in the supernatant of geKRMs (**D**) and M(–) mBMDMs (**E**) was analyzed by ELISA ($n = 3$ for each; mean ± SD; $^*p < 0.05$ and $^{**}p < 0.01$ vs. WT). **F** M(–) were treated with dsDNA with or without 10 μg/mL cycloheximide (CHX). Cytokine release was analyzed ($n = 3$ for each; mean ± SD; $^*p < 0.05$ and $^{**}p < 0.01$. $^{\#\#}p < 0.01$ vs. WT). **G** M(–) were treated with dsDNA with or without H151. Cytokine release was analyzed ($n = 3$ for each; mean ± SD; $^{**}p < 0.01$. $^{\#}p < 0.05$ and $^{\#\#}p < 0.01$ vs. WT).

(Forward, 5′-CAGGTGTGGGCTCAGGTAGT-3′, reverse, 5′-TGTGGTG AGCTGAAAGGTGA-3′), *Cd68* (Forward, 5′-CTTCCCACAGGCAGCAC AG-3′, reverse, 5′-AATGATGAGAGGCAGCAAGAGG-3′), *Cxcl10* (For-ward, 5′-ACGTGTTGAGATCATTGCCA-3′, reverse, 5′-GGCTCTCTGC TGTCCATCCAT-3′), *Cxcr3* (Forward, 5′-CGCAGCCCAAGTCCTAACAC ACT-3′, reverse, 5′-CTGGCAGCAAAGTTACGGGTAAG-3′), *Gapdh* (Forward, 5′-TGTGTCCGTCGTGGATCTGA-3′, reverse, 5′-TTGCTGTT GAAGTCGCAGGAG-3′), *Hacvr1* (Kim1, forward, 5′-CTGGAATGGCA CTGTGACATCC-3′, reverse, 5′-GCAGATGCCAACATAGAAGCCC-3′), *Ifnb1* (Forward, 5′-GCCTTTGCCATCCAAGAGATGC-3′, reverse, 5′-AC ACTGTCTGCTGGTGGAGTTC-3′), *Lcn2* (Ngal, forward, 5′-GAAATATG CACAGGTATCCTC-3′, reverse, 5′-GTAATTTTGAAGTATTGCTTGTTT-3′), *Tnfa* (Forward,5′-AAGCCTGTAGCCCACGTCGTA-3′, reverse, 5′-GGCACCACTAGTTGGTTGTCTTTG-3′), *Il1a* (Forward,5′-TCAACCAAA CTATATATCAGGATGTGG-3′, reverse, 5′-CGAGTAGGCATACATGTC AAATTTTAC-3′), and *Il18* (Forward,5′-CAGGCCTGACATCTTCTGCA A-3′, reverse, 5′-TCTGACATGGCAGCCATTGT-3′).

Thermal Cycler Dice Real-Time Systems II (Takara Bio Inc., Shiga, Japan) was used for real-time RT-PCR to analyze mRNA expression. The expression levels of each gene were normalized to *Gapdh* or *Actb* by using the $\Delta\Delta C_T$ comparison method.

Histology and immunostaining

The kidneys were fixed with 10% formalin and embedded in paraffin. Frozen samples were stored in OCT compound at −80 °C. The tissue sections (5 μm-thick) were subjected to Periodic-Acid Schiff (PAS) staining, Masson's Trichrome staining, and Picrosirius red staining using standard protocols. For measurement of fibrosis, Picrosirius red-stained samples were assessed in five random fields under polarized microscopy (Olympus IX73, Tokyo, Japan) and CellSens software (ver.1.12, Olympus, Tokyo, Japan). Tubular injury was assessed on PAS samples in terms of necrotic lysis, tubular dilatation, tubular brush border loss, cast formation, and sloughing of cellular debris into the tubular lumen. The injury score was blindly determined by the same nephrologist as described previously [8, 53], according to the following grades: normal as grade 0; <25% as grade 1; 25–49% as grade 2; 50–74% as grade 3; and ≥75% as grade 4.

Immunohistochemistry (IHC) of paraffin-embedded sections was performed to evaluate KIM-1, F4/80 and αSMA in the kidney. Kidney sections were deparaffinized, boiled in Target Retrieval Solution (Dako, Carpinteria, CA, USA), blocked with a 2% normal goat serum, and reacted to primary antibodies overnight. Anti-F4/80 (BioRad), Arginase-1 (D4E3M, Cell Signaling, Danvers, MA, USA) or TIM-1/KIM-1 antibody (R&D Systems, Minneapolis, MN, USA)-treated sections were incubated with Histofine Simple Stain MAX PO (Nichirei Bioscience, Tokyo, Japan), followed by DAB substrate kit (Vector Laboratories, Burlingame, CA, USA); anti-Actin-αSMA-AP (Sigma Aldrich, St. Louis, MO, USA)-treated sections were incubated with Alkaline Phosphatase Substrate-Vector Red (Vector Laboratories, Burlingame, CA, USA). All sections were counterstained with Hematoxylin. Species-matched immunoglobulin G (IgG) was used as a negative control for primary antibodies. PAS, Picrosirius red, and IHC-stained sections were digitized using a microscope (FSX-100; Olympus). Fibrotic area and IHC-positive areas were quantified using ImageJ (Fiji, National Institutes of Health, USA).

For immunofluorescent staining, paraffin-embedded sections were deparaffinized, antigen retrieved, blocked, and incubated overnight with primary antibodies of CD206, CXCR3 (BioLegend), F4/80 (BioRad), pTBK1 (S172), cleaved Casp-3 (Cell Signaling). Sections were then incubated with fluorescent-conjugated secondary antibodies (Thermo Fischer Scientific, Waltham, MA) and the nuclear stain DAPI (Wako, Osaka, Japan). For co-staining with the terminal deoxynucleotidyl transferase dUTP nick end labelling (TUNEL), an In Situ Cell Death Detection kit (Roche, Basel, Switzerland) was used. For immunofluorescent cell staining, cells were seeded on collagen-coated coverslips. Cells were fixed with 4% paraformaldehyde (PFA), permeabilized with 0.1% Triton, blocked, and incubated with primary antibodies for CD11b or pTBK1 for an hour. Cells were then reacted to the secondary antibodies conjugated with fluorochromes. Fluorescein-conjugated *Lotus tetragonolobus* lectin (LTL) (Vector Laboratories), Alexa 568-conjugated Phalloidin, and DAPI were used for co-staining for the apical membrane of proximal tubular cells, F-actin, and nuclei, respectively. Images of the stained sections were digitized and analyzed using an FV1000 microscope (Olympus).

Immunoblotting

Total protein lysates were prepared from kidneys using RIPA lysis buffer (20 mM Tris, 2.5 mM EDTA, 1% Triton X, 10% glycerol, 1% deoxycholic acid, 0.1% SDS, 50 mM NaF, and 10 mM $Na_4P_2O_7{\cdot}10H_2O$) with protease inhibitors. Protein lysates from cells were obtained by directly adding 5x Laemmli sample buffer to wells containing both cells and supernatants to prevent the loss of dead cells. Protein samples were denatured by boiling at 95 °C for 8 min under reducing conditions and then subjected to SDS-PAGE. The protein bands were transferred to nitrocellulose membranes. The membranes were blocked for an hour at RT with 5% skim milk or BSA buffer and then reacted to the primary antibodies at 4 °C overnight, followed by incubation for an hour with the secondary antibodies conjugated with horse-radish peroxidase (HRP). Western blot Quant HRP substrate or Ultra-Sensitive HRP substrate (Takara Bio Inc.) was used to detect the bands with an Amersham imager 680 (Cytiva, MA, USA). β-actin was used as an internal control for the amount of protein loaded. Primary antibodies against mouse Aim2 (Cell Signaling), GSDMD (Adipogen), cleaved GSDMD (Cell Signaling), Caspase-1 (p20, Adipogen), IL-1β (R&D), pIRF3 (Ser 396), IRF3, pTBK1(Ser 172), TBK1, STING, p-p65 (Ser 536, Cell Signaling), p65 (Santa Cruz Biotechnology, Dallas, TX, USA), HMGB1 (Gene Tex, Irvine, CA, USA) and β-actin (Sigma) were used. Full length original immunoblots are provided in Supplementary Source File 1.

Flow cytometry

Flow cytometric analysis was conducted as described previously [7]. In brief, mouse kidney was harvested, minced into small pieces, and digested in collagenase D mixture (1 mg/mL collagenase D, 40 ng/mL DNase-I, and 5 mM $MgCl_2$ in RPMI-1640) for 40 min at 37 °C. The tissue was pipetted until it became a homogenous suspension and filtered through a 40-μm cell strainer. After the tissue was incubated in ACK buffer to lyse red blood cells, cells were suspended with 40% Percoll and carefully overlaid on 80% Percoll. After centrifugation, kidney

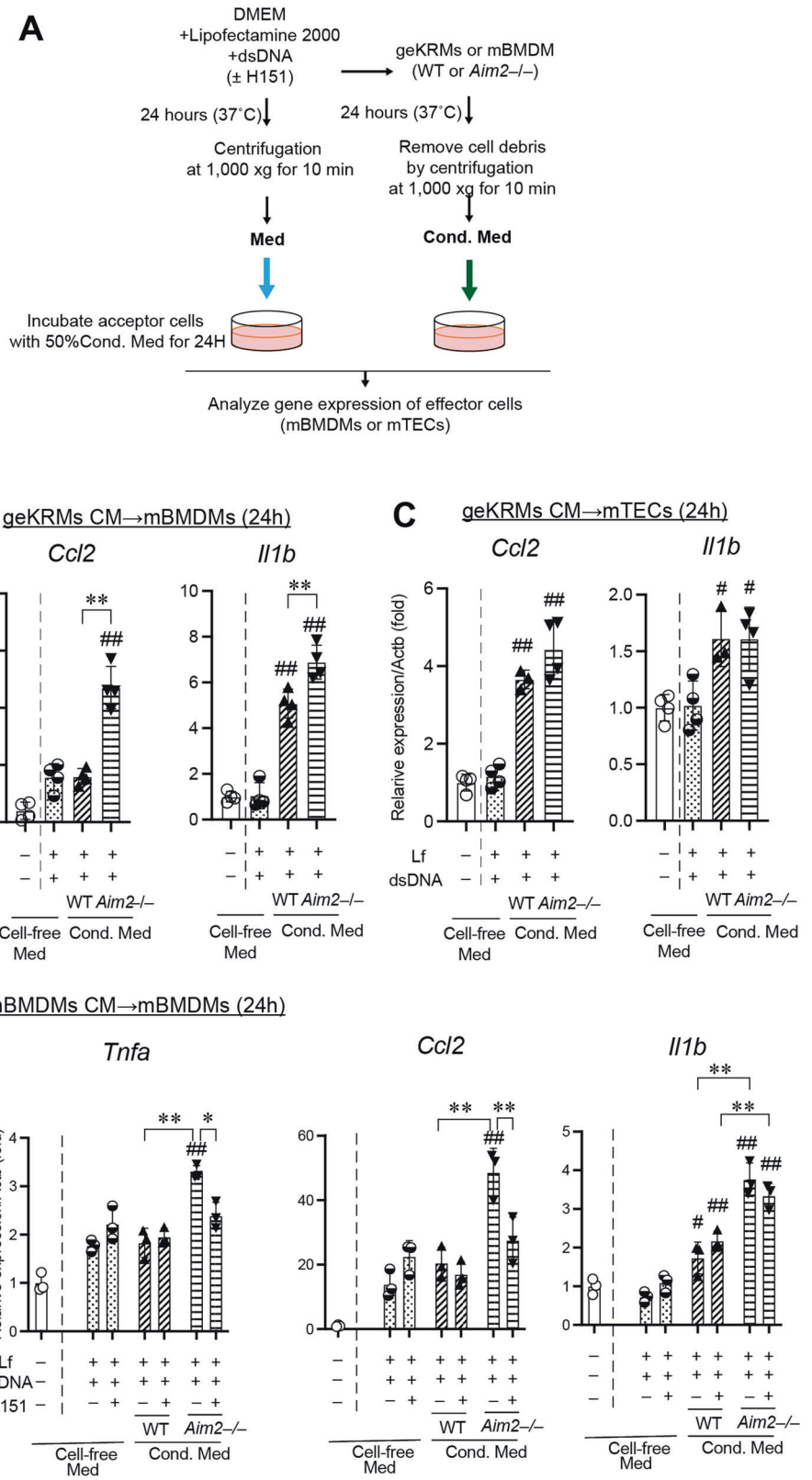

Fig. 7 Escape from AIM2 pyroptosis propagates inflammation to surrounding cells. A The experimental design is shown. **B** The cytokine mRNA levels of acceptor macrophages after incubation in conditioned medium (Cond. Med) were analyzed by real-time RT-PCR. **C** The cytokine mRNA levels of acceptor mTECs after incubation in Cond. Med were analyzed by real-time RT-PCR. **D** M(–) mBMDMs were treated with 2 μg/mL poly (dA:dT) with or without H151 for 24 h. Collected Cond. Med was added to acceptor mBMDMs and incubated for 24 h. The cytokine mRNA levels of acceptor mBMDMs were analyzed by real-time RT-PCR. Note that cell-free control medium containing dsDNA-Lipofectamine complex scarcely affected the acceptor cell response, confirming that the carry-over of dsDNA in conditioned medium was negligible ($n = 3$ for each; mean ± SD; $^{*}p < 0.05$ and $^{**}p < 0.01$. $^{\#}p < 0.05$ and $^{\#\#}p < 0.01$ vs. controls incubated with Lipofectamine/dsDNA-containing cell-free medium).

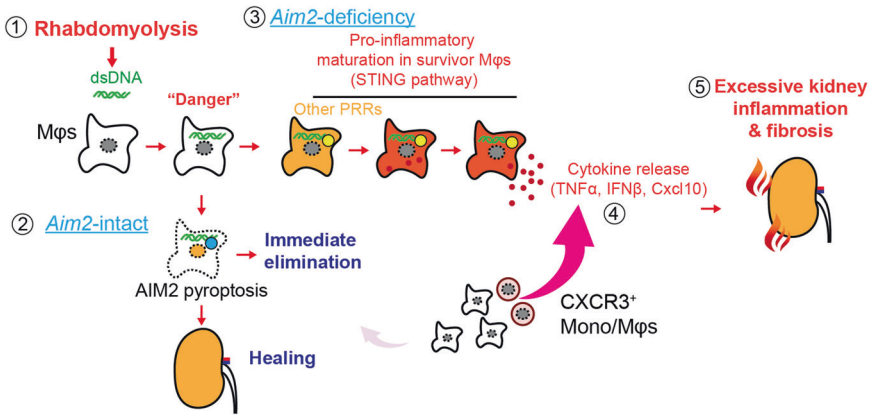

Fig. 8 Proposed mechanism of immune elimination by AIM2 pyroptosis. 1: Detrimental muscular injury and/or acute tubular necrosis (ATN) in the kidney release endogenous dsDNA, and macrophages (Mφs) in the kidney take up dsDNA as a "danger signal". 2: Macrophages carrying AIM2 engage AIM2 pyroptosis upon dsDNA binding, resulting in the rapid elimination of macrophages. Properly regulated inflammation renders normal kidney healing. 3: Under *Aim2*-deficiency, macrophages escape from the rapid cell death machinery and mature alternate STING pathways leading to cytokine release. 4: Secreted cytokines such as TNFα, IFNβ, and CXCL10 attract $CXCR3^+$ monocytes(Mono)/Mφs. 5: STING-dependent cytokines develop excessive inflammation and abnormal fibrosis in the kidney, resulting in an AKI-to-CKD transition.

leukocytes were layered between Percoll. Leukocytes were labelled with the following antibodies: FITC-conjugated anti-CD11b (BD Biosciences, CA, USA), 7-AAD (BD Biosciences), Brilliant Violet 421-conjugated anti-F4/80 (BioLegend), Brilliant Violet 510 -conjugated anti-CD45 (BD Biosciences). mBMDMs in vitro were labeled by an anti-CD206 antibody (BioLegend) followed by an Alexa-647-conjugated secondary antibody (Thermo). BD FACSVerse (BD Biosciences) was used for analyzing immunophenotypes, and FlowJo software (ver.10, Tree Star, Inc., Ashland, OR, USA) was used to analyze the data.

Serum chemistry

Mouse serum BUN, creatinine, and LDH levels were analyzed with a Fuji Dri-Chem analyzer (Fujifilm, Tokyo, Japan).

Picogreen assay

Mouse blood was collected from the jugular vein under anesthesia before and after glycerol injection. The plasma dsDNA level was measured by Quant-iT PicoGreen dsDNA Reagent and kits (Thermo Fisher Scientific) according to the manufacturer's protocol. Fluorescence was measured using a SPARK 10 M multimode microplate reader (TECAN, Switzerland).

Live cell imaging

WT and *Aim2*–/– mBMDMs and WT geKRMs were grown on collagen-coated glass-bottom dishes in serum-free RPMI1640 with Hoechst33342 and Sytox orange (Thermo Fisher Scientific), and induced to undergo pyroptosis with poly (dA:dT) using Lipofectamine 2000. Images were taken using a fluorescent microscope FV1000 over a 2.5 h time course at 37 °C in a 5% CO_2 atmosphere.

BrdU incorporation analysis

Glycerol-injected mice received a single intraperitoneal injection of 100 mg/kg of 5-bromo-2-deoxyuridine (BrdU, Tocris Biosciences, Minneapolis, MN, USA) 24 h before sacrifice. After the kidney was harvested, samples were fixed and embedded in paraffin. Next, 3-μm paraffin-embedded sections were deparaffinized, antigen-retrieved, blocked, and incubated overnight with a primary antibody for BrdU (MBL). The following steps were similar to the immunofluorescent staining method mentioned above.

ELISA

The levels of TNFα, IFNβ, IL-1β, IL-1α, IL-18, and CCL2 in cell supernatants and/or tissues were measured using a mouse ELISA kit (R&D Systems) according to the manufacturer's instructions.

Statistics

Data are expressed as mean ± SD from at least three independent experiments. All measurements were taken from distinct samples, and no data were excluded. Sample sizes were based in standard protocols in the field. First, a normality test and an *F* test were performed on all data. If the data showed a normal distribution, a paired or unpaired two-tailed *t*-test was used to compare the two groups. For comparisons between multiple groups, the significance of differences in between-group means was determined by one-way analysis of variance (ANOVA) combined with the Tukey–Kramer test or Dunnett post-hoc test. Multiple groups with repeated measurements were analyzed with two-way ANOVA with Šidák' s post-hoc test. All analyses were performed using GraphPad Prism version 9 (GraphPad Software Inc., San Diego, CA, USA). A p value of <0.05 was considered statistically significant.

DATA AVAILABILITY

The data generated in this study and additional supporting data are available from corresponding authors on reasonable request.

REFERENCES

1. Bosch X, Poch E, Grau JM. Rhabdomyolysis and Acute Kidney Injury. New Engl J Medicine. 2009;361:62–72.
2. McMahon GM, Zeng X, Waikar SS. A risk prediction score for kidney failure or mortality in Rhabdomyolysis. JAMA Intern Med. 2013;173:1821.
3. Candela N, Silva S, Georges B, Cartery C, Robert T, Moussi-Frances J, et al. Short- and long-term renal outcomes following severe rhabdomyolysis: a French multicenter retrospective study of 387 patients. Annals of Intensive Care. 2020;10. https://doi.org/10.1186/s13613-020-0645-1.
4. Okubo K, Kurosawa M, Kamiya M, Urano Y, Suzuki A, Yamamoto K, et al. Macrophage extracellular trap formation promoted by platelet activation is a key mediator of rhabdomyolysis-induced acute kidney injury. Nat Med. 2018;24:232.
5. Rathinam VAK, Jiang Z, Waggoner SN, Sharma S, Cole LE, Waggoner L, et al. The AIM2 inflammasome is essential for host defense against cytosolic bacteria and DNA viruses. Nat Immunol. 2010;11:395–402.
6. Hornung V, Ablasser A, Charrel-Dennis M, Bauernfeind F, Horvath G, Caffery DR. AIM2 recognizes cytosolic dsDNA and forms a caspase-1-activating inflammasome with ASC. Nature. 2009;458:514–8.
7. Komada T, Chung H, Lau A, Platnich JM, Beck PL, Benediktsson H, et al. Macrophage uptake of necrotic cell DNA activates the AIM2 inflammasome to regulate a proinflammatory phenotype in CKD. J Am Soc Nephrol. 2018;29:1165.
8. Komada T, Usui F, Kawashima A, Kimura H, Karasawa T, Inoue Y, et al. Role of NLRP3 inflammasomes for rhabdomyolysis-induced acute kidney injury. Scientific Rep. 2015;5:10901.

9. Dempsey A, Bowie AG. Innate immune recognition of DNA: a recent history. Virology. 2015;479-480:146–52.
10. Unterholzner L. The interferon response to intracellular DNA: why so many receptors? Immunobiology. 2013;218:1312–21.
11. Lauková L, Konečná B, Janovičová Ľ, Vlková B, Celec P. Deoxyribonucleases and their applications in biomedicine. Biomolecules. 2020;10:1036.
12. Chung H, Komada T, Lau A, Chappellaz M, Platnich JM, de Koning HD, et al. AIM2 suppresses inflammation and epithelial cell proliferation during glomerulonephritis. J Immunol (Baltim, Md: 1950). 2021;207:2799–812.
13. Panchanathan R, Shen H, Duan X, Rathinam VAK, Erickson LD, Fitzgerald KA, et al. Aim2 deficiency in mice suppresses the expression of the inhibitory fcγ receptor (FcγRIIB) through the Induction of the IFN-Inducible p202, a Lupus Susceptibility Protein. J Immunol. 2011;186:6762–70.
14. Nakaya Y, Lilue J, Stavrou S, Moran EA, Ross SR. AIM2-like receptors positively and negatively regulate the interferon response induced by cytosolic DNA. mBio. 2017;8:e00944-17.
15. Guzzi F, Cirillo L, Roperto RM, Romagnani P, Lazzeri E. Molecular mechanisms of the acute kidney injury to chronic kidney disease transition: an updated view. Int J Mol Sci. 2019;20:4941.
16. Ostermann M, Bellomo R, Burdmann EA, Doi K, Endre ZH, Goldstein SL, et al. Controversies in acute kidney injury: conclusions from a Kidney Disease: Improving Global Outcomes (KDIGO) Conference. Kidney Int. 2020;98:294–309.
17. Sato Y, Yanagita M. Immune cells and inflammation in AKI to CKD progression. Am J Physiol-Ren Physiol. 2018;315:F1501.
18. Yoo KD, Cha R, Lee S, Kim JE, Kim KH, Lee JS, et al. Chemokine receptor 5 blockade modulates macrophage trafficking in renal ischaemic-reperfusion injury. J Cell Mol Med. 2020;24:5515.
19. Zhou J, Tang PCY, Qin L, Gayed PM, Li W, Skokos EA, et al. CXCR3-dependent accumulation and activation of perivascular macrophages is necessary for homeostatic arterial remodeling to hemodynamic stresses. J Exp Med. 2010;207:1951–66.
20. Belliere J, Casemayou A, Ducasse L, Zakaroff-Girard A, Martins F, Iacovoni JS, et al. Specific macrophage subtypes influence the progression of Rhabdomyolysis-induced kidney injury. J Am Soc Nephrol. 2014;26:1363.
21. Nagata S, Tanaka M. Programmed cell death and the immune system. Nat Rev Immunol. 2017;17:333.
22. Tzeng T-C, Schattgen S, Monks B, Wang D, Cerny A, Latz E, et al. A fluorescent reporter mouse for inflammasome assembly demonstrates an important role for cell-bound and free ASC specks during in vivo infection. Cell Rep. 2016;16:571–82.
23. Balka KR, Louis C, Saunders TL, Smith AM, Calleja DJ, D'Silva DB, et al. TBK1 and IKKε act redundantly to mediate STING-induced NF-κB responses in myeloid cells. Cell Rep. 2020;31:107492.
24. Yum S, Li M, Fang Y, Chen ZJ. TBK1 recruitment to STING activates both IRF3 and NF-κB that mediate immune defense against tumors and viral infections. Proc Natl Acad Sci. 2021;118:e2100225118.
25. Zahid A, Ismail H, Li B, Jin T. Molecular and structural basis of DNA sensors in antiviral innate immunity. Front Immunol. 2020;11:613039.
26. Corrales L, Woo S-R, Williams JB, McWhirter SM, Gajewski TF. Antagonism of the STING pathway via activation of the AIM2 inflammasome by intracellular DNA. J Immunol. 2016;196:3191.
27. Konno H, Konno K, Barber Glen N. Cyclic dinucleotides trigger ULK1 (ATG1) phosphorylation of STING to prevent sustained innate immune signaling. Cell. 2013;155:688–98.
28. Prabakaran T, Bodda C, Krapp C, Zhang B, Christensen MH, Sun C, et al. Attenuation of cGAS - STING signaling is mediated by a p62/ SQSTM1-dependent autophagy pathway activated by TBK1. The EMBO J. 2018;37:e97858.
29. Haag SM, Gulen MF, Reymond L, Gibelin A, Abrami L, Decout A, et al. Targeting STING with covalent small-molecule inhibitors. Nature. 2018;559:269–73.
30. Galluzzi L, Vitale I, Aaronson SA, Abrams JM, Adam D, Agostinis P, et al. Molecular mechanisms of cell death: recommendations of the Nomenclature Committee on Cell Death 2018. Cell Death Differ. 2018;25:486–41.
31. Kayagaki N, Kornfeld OS, Lee BL, Stowe IB, O'Rourke K, Li Q, et al. NINJ1 mediates plasma membrane rupture during lytic cell death. Nature. 2021;591:131–36.
32. Lammert CR, Frost EL, Bellinger CE, Bolte AC, McKee CA, Hurt ME, et al. AIM2 inflammasome surveillance of DNA damage shapes neurodevelopment. Nature. 2020;580:647–52.
33. Yan S, Shen H, Lian Q, Jin W, Zhang R, Lin X, et al. Deficiency of the AIM2–ASC signal uncovers the STING-driven overreactive response of type I IFN and reciprocal depression of protective IFN-γ immunity in mycobacterial infection. J Immunol. 2017;200:1016–26.
34. Wang Y, Ning X, Gao P, Wu S, Sha M, Lv M, et al. Inflammasome Activation Triggers Caspase-1-Mediated Cleavage of cGAS to Regulate Responses to DNA Virus Infection. Immunity. 2017;46:393–404.
35. Su S, Zhao J, Xing Y, Zhang X, Liu J, Ouyang Q, et al. Immune checkpoint inhibition overcomes ADCP-induced immunosuppression by macrophages. Cell. 2018;175:442–57.e23.
36. Banerjee I, Behl B, Mendonca M, Shrivastava G, Russo AJ, Menoret A, et al. Gasdermin D restrains type I interferon response to cytosolic DNA by disrupting ionic homeostasis. Immunity. 2018;49:413–26.e5.
37. Panchanathan R, Duan X, Shen H, Rathinam VAK, Erickson LD, Fitzgerald KA, et al. Aim2 deficiency stimulates the expression of IFN-inducible Ifi202, a Lupus susceptibility murine gene within the Nba2 autoimmune susceptibility locus. J Immunol. 2010;185:7385–93.
38. Storek KM, Gertsvolf NA, Ohlson MB, Monack DM. cGAS and Ifi204 cooperate to produce type I IFNs in response to Francisella infection. J Immunol. 2015;194:3236–45.
39. Ma C, Li S, Hu Y, Ma Y, Wu Y, Wu C, et al. AIM2 controls microglial inflammation to prevent experimental autoimmune encephalomyelitis. J Exp Med. 2021;218: e20201796.
40. Tsuchiya K, Nakajima S, Hosojima S, Thi Nguyen D, Hattori T, Manh Le T, et al. Caspase-1 initiates apoptosis in the absence of gasdermin D. Nat Commun. 2019;10:2091.
41. Aizawa E, Karasawa T, Watanabe S, Komada T, Kimura H, Kamata R, et al. GSDME-dependent incomplete pyroptosis permits selective IL-1α release under caspase-1 inhibition. iScience. 2020;23:101070.
42. Chung H, Vilaysane A, Lau A, Stahl M, Morampudi V, Bondzi-Simpson A, et al. NLRP3 regulates a non-canonical platform for caspase-8 activation during epithelial cell apoptosis. Cell Death Differ. 2016;23:1331–46.
43. Chun J, Chung H, Wang X, Barry R, Taheri ZM, Platnich JM, et al. NLRP3 localizes to the tubular epithelium in human kidney and correlates with outcome in IgA nephropathy. Scientific Rep. 2016;6:24667.
44. Komada T, Usui F, Shirasuna K, Kawashima A, Kimura H, Karasawa T, et al. ASC in renal collecting duct epithelial cells contributes to inflammation and injury after unilateral ureteral obstruction. Am J Pathol. 2014;184:1287–98.
45. Gauer S, Sichler O, Obermüller N, Holzmann Y, Kiss E, Sobkowiak E, et al. IL-18 is expressed in the intercalated cell of human kidney. Kidney Int. 2007;72:1081–7.
46. Mizuno-Iijima S, Ayabe S, Kato K, Matoba S, Ikeda Y, Dinh TTH, et al. Efficient production of large deletion and gene fragment knock-in mice mediated by genome editing with Cas9-mouse Cdt1 in mouse zygotes. Methods. 2021;191:23–31.
47. Yamamoto M, Yaginuma K, Tsutsui H, Sagara J, Guan X, Seki E, et al. ASC is essential for LPS-induced activation of procaspase-1 independently of TLR-associated signal adaptor molecules. Genes Cells. 2004;9:1055–67.
48. Kuida K, Lippke J, Ku G, Harding M, Livingston D, Su M, et al. Altered cytokine export and apoptosis in mice deficient in interleukin-1 beta converting enzyme. Science. 1995;267:2000–03.
49. Tsutsui H, Kayagaki N, Kuida K, Nakano H, Hayashi N, Takeda K, et al. Caspase-1-independent, Fas/Fas ligand-mediated IL-18 secretion from macrophages causes acute liver injury in mice. Immunity. 1999;11:359–67.
50. Kayagaki N, Stowe IB, Lee BL, O'Rourke K, Anderson K, Warming S, et al. Caspase-11 cleaves gasdermin D for non-canonical inflammasome signalling. Nature. 2015;526:666–71.
51. Singh AP, Muthuraman A, Jaggi AS, Singh N, Grover K, Dhawan R. Animal models of acute renal failure. Pharmacol Rep. 2012;64:31–44.
52. White LR, Blanchette JB, Ren L, Awn A, Trpkov K, Muruve DA. The characterization of α5-integrin expression on tubular epithelium during renal injury. Am J Physiol-Renal Physiol. 2007;292:F567–F576.
53. Wei Q, Hill WD, Su Y, Huang S, Dong Z. Heme oxygenase-1 induction contributes to renoprotection by G-CSF during rhabdomyolysis-associated acute kidney injury. Am J Physiol-Renal Physiol. 2011;301:F162–F170.

ACKNOWLEDGEMENTS

We are grateful to Naoko Sugaya, Masako Sakurai, and Rumiko Ochiai for their technical assistance. We thank Dr. Kate Schroder, Dr. Hiroko Tsusui, and Dr. Shun'ichiro Taniguchi for providing *Gsdmd*–/–, *Casp1/11*–/–, and *Asc*–/– mice, respectively.

AUTHOR CONTRIBUTIONS

CB and TK performed most of the experiments and data analysis and wrote the manuscript. CB, TK, and MT designed the study concept. TK, NY, AS, and TM performed the experiments and analyzed data. MT oversaw the entire project, analyzed data, and wrote the manuscript. All of the authors reviewed the manuscript.

FUNDING

This study was supported by the Japan Society for the Promotion of Science (JSPS) through Grants-in-Aid for Scientific Research (C), (21K08114, MT; 21K06875, TK), a Grant-in-Aid for Research Activity Start-up (19K21319, TK), a Grant-in-Aid for

Early-Career Scientists (20K17290, TK), a JMU Young Investigator Award (TK), and a JMU Graduate Student Start-up Award and Student Research Award (CB).

COMPETING INTERESTS

The authors declare no competing interests.

ETHICAL APPROVAL

No experiments involving human subjects were performed in this study. All animal experiments were approved by the Use and Care of Experimental Animals Committee of Jichi Medical University (permission number 21021-01) and carried out following Jichi Medical University guidelines.

ADDITIONAL INFORMATION

Supplementary information The online version contains supplementary material available at https://doi.org/10.1038/s41418-022-01033-9.

Correspondence and requests for materials should be addressed to Takanori Komada or Masafumi Takahashi.

Reprints and permission information is available at http://www.nature.com/reprints

Publisher's note Springer Nature remains neutral with regard to jurisdictional claims in published maps and institutional affiliations.